Research Letter **DOI: 10.15541/jim20250396**

Deactivation Mechanism of Pd Only Three-way Catalysts under Aging Temperature Gradient

LIU Xuzi[1], SONG Zhaohua[1], ZENG Lu[1], QU Li[2], JIAO Yi[1], JIANG Fajun[3], LI Dacheng[3], YAN Huicheng[4], WANG Jianli[2], CHEN Yaoqiang[2]

(1. Institute of New Energy and Low-Carbon Technology, Sichuan University, Chengdu 610064, China; 2. College of Chemistry, Sichuan University, Chengdu 610064, China; 3. SINOTECH Company Limited, Chengdu 611731, China; 4. Sichuan Shutai Chemical Technology Co., Ltd., Suining 629300, China)

Abstract: Pd/CZA catalyst composed of third-generation oxygen storage material CeO_2-ZrO_2-Al_2O_3 (CZA) loaded only with Pd represents a practical three-way catalyst (TWC) owing to its exceptional pollutant conversion efficiency and sintering resistance. Although the thermal degradation mechanism of Pd-based TWC has been confirmed to be closely associated with Pd sintering and the weakening of metal-support interaction (MSI), a systematic investigation into its thermal aging behavior under an extreme high temperature gradient remains necessary. A series of Pd/CZA catalysts aged at 800–1000 ℃ were prepared in this study and their thermal degradation was systematically explored, presenting a pioneering investigation into the evolution pattern of the microchemical state of Pd with aging temperature gradient. The correlation among the microchemical state of Pd, MSI and aging resistance was evaluated through different characterization techniques. The results showed that catalytic activity exhibited a nonlinear decay with increasing aging temperature. Catalytic performance declined sharply in the range of 850–900 ℃, with increases of 26–40 ℃ and 39–67 ℃ for T_{50} and T_{90} (the temperatures at which the pollutant conversions are 50% and 90%, respectively) of carbon monoxide (CO), nitric oxide (NO) and hydrocarbon (HCs), while showed little variation within the range of 900–1000 °C. The underlying reason for this sharp decline in activity is an abrupt transformation in the microchemical state of Pd. When the aging temperature increases to 900 °C, the Pd–O–Ce bond is weakened, which compromises the MSI. Consequently, Pd particles become unanchored, undergo rapid sintering and growth, and exhibit diminished capabilities for adsorbing and activating both reactants and oxygen.

Keywords: temperature gradient; thermal aging; Pd–O–Ce bond; metal-support interaction; three-way catalyst

Stringent emission regulations, exemplified by China VI-b, necessitate TWCs for gasoline vehicle exhaust purification that demonstrate high catalytic activity and long-term stability under demanding high-temperature conditions[1-2]. TWCs must efficiently convert CO, HCs, and NO_x simultaneously, with their durability directly impacting the overall performance of the exhaust emission system[3]. Noble metals and support materials are the two core constituents of TWCs. Typically, TWCs utilize platinum group metals (PGMs) as primary active components. Among these, Pd has increasingly supplanted the traditional Pt-Rh system as the preferred option for contemporary TWCs due to its superior low-temperature redox activity, resistance to sulfur poisoning, and relatively lower cost[4-5]. Meanwhile, the catalytic activity and long-term stability of TWCs rely on redox properties and stability of the support. CZA composite oxides have emerged as optimal TWC support materials

收稿日期：2025-10-10；收到修改稿日期：2025-12-24；网上出版日期：xxxx-xx-xx
基金项目：国家科技重大专项(2024ZD0606500)；国家自然科学基金(22472108)
Advanced Materials-National Science and Technology Major Project (2024ZD0606500); National Natural Science of China (22472108)
作者简介：刘栩孜(2000–)，女，硕士研究生. E-mail: lxz@stu.scu.edu.cn
LIU Xuzi (2000–), female, Master candidate. E-mail: lxz@stu.scu.edu.cn
通信作者：焦 毅，副研究员. E-mail: jiaoyiscu@163.com
JIAO Yi, associate professor. E-mail: jiaoyiscu@163.com

owing to their high specific surface area, exceptional oxygen storage capacity (OSC), and robust anchoring effect for noble metals[6-7]. Notably, the CeO_2-ZrO_2 solid solution within CZA governs the redox cycle by facilitating the formation of reversible oxygen vacancy[8-9], while Al_2O_3 contributes a high specific surface area to achieve a highly dispersed active site configuration[10-11]. In comparison to single-support Pd-based TWCs, the Pd/CZA catalyst serves as a TWC more closely aligned to actual industrial operating conditions.

The long-term performance of Pd/CZA is limited by the sintering of active phases and structural degradation of the support during thermal aging. Studies have shown that the sintering of the Pd active component after aging is the main cause of deactivation in TWCs. Regarding the sintering of noble metal, the most common explanations are the mechanisms of particle migration and coalescence (PMC) and Oswald ripening (OR), which involve Brownian-like diffusion of surface metal particles resulting in collision and growth, and the dissolution and redeposition of surface metal atoms onto larger particles, respectively[12]. The loading amount of noble metal affects the high-temperature sintering of Pd. Vedyagin *et al*.[13] observed Pd agglomeration during thermal aging at 1000 ℃, beginning at 1% (in mass) Pd loading. The sintering of Pd also depends on the operating atmosphere. Muta *et al*.[14] found that in the lean atmosphere, Pd in Pd/Al_2O_3 was oxidized to PdO while the rich atmosphere had little effect on Pd. Unlike Rh/Al_2O_3, the effect of aging temperature on the deactivation of Pd/Al_2O_3 was more pronounced than that of the atmosphere. Additionally, the phase transformation of γ-Al_2O_3 to α-Al_2O_3 and the phase separation of CeO_2-ZrO_2 solid solution in the CZA support contribute to a decline in active sites under the extreme high temperatures generated by gasoline engines[5, 15-16]. For example, Cheng *et al*.[17] observed that dry thermal aging resulted in increased separation of CeO_2 from the CeO_2-ZrO_2 solid solution compared to hydrothermal aging, leading to agglomeration of noble metal particles. Fujiwara *et al*.[18] developed a model for the aging process of Pd/CeO_2-ZrO_2 and Pd/Al_2O_3, proposing that the main factor causing the deactivation of Pd/CZ is the loss in the number of Pd_b (circular periphery of the Pd/CZ interface) sites, while the main factor contributing to the deactivation of Pd/Al_2O_3 is the decrease in the relative content of isolated Pd^{2+}[19]. Additionally, dynamic operating conditions with temperature fluctuations induce thermal stress, accelerating the degradation of MSI and interfacial bonds[20].

The microchemical environment is the specific physical and chemical surroundings of the catalytic sites[21]. In this context, microchemical state describes the condition of the noble metal in this specific microchemical environment. Although numerous studies have been devoted to investigating the deactivation behavior of Pd-based catalysts, the dynamic evolution of their microchemical state under high-temperature conditions and the underlying microscopic mechanisms remain poorly understood. This knowledge gap represents a critical bottleneck for the rational design of high-stability catalysts. Notably, in practical operating conditions, thermal aging of catalysts is a complex process affected by multiple temperatures rather than a single value. Meanwhile, the Tammann and Hüttig temperatures, indicative of two sintering mechanisms' initiation, demonstrate distinct mathematical and physical relationships with the metal's melting point[22]. In summary, investigating the aging behaviors and mechanisms of Pd-based TWCs under a high-temperature gradient not only enhances an understanding of the thermal degradation mechanism, but also provides a theoretical basis for designing highly stable catalysts.

In this study, Pd/CZA was selected as the research object, and the microchemical state of Pd was focused to investigate the thermal aging behaviors of Pd/CZA catalysts under a high-temperature gradient of 800–1000 ℃, which represents the harsh conditions in gasoline vehicle exhaust environments. Influence of the support on the catalytic performance was minimized by employing the 1000 ℃-aged CZA as the support. Using various characterizations, the effect of temperature on the changes in Pd particle size, chemical state, and redox properties was investigated.

1 Experimental

Pd/CZA were prepared by incipient wet impregnation, then aged at 800, 850, 900, 950, and 1000°C for 5 h, and named as Pd/CZA-800, Pd/CZA-850, Pd/CZA-900, Pd/CZA-950, and Pd/CZA-1000, respectively. The detailed preparation, characterization procedures and method of activity tests are described in the Supporting materials.

2 Results and discussion

2.1 Catalytic performance

Fig. 1 and Table 1 illustrate the catalytic performance of Pd/CZA catalysts after various high-temperature aging treatments. The general trend indicates a decline in catalysts activity as the aging temperature increases,

consistent with the conventional understanding that elevated temperatures promote sintering and agglomeration of noble metal particles, leading to gradual deactivation[23-24]. Notably, a significant drop in activity is observed for the catalyst aged at 900 ℃ compared to that aged at 850 ℃. Variations in T_{50} and T_{90} values for CO, NO and HCs range from 26 to 40 ℃ and from 39 to 67 ℃, respectively. Conversely, the disparity in activity between catalysts aged at 800 and 850 ℃ is minimal, and the distinctions among those aged at 900, 950 and 1000 ℃ are negligible.

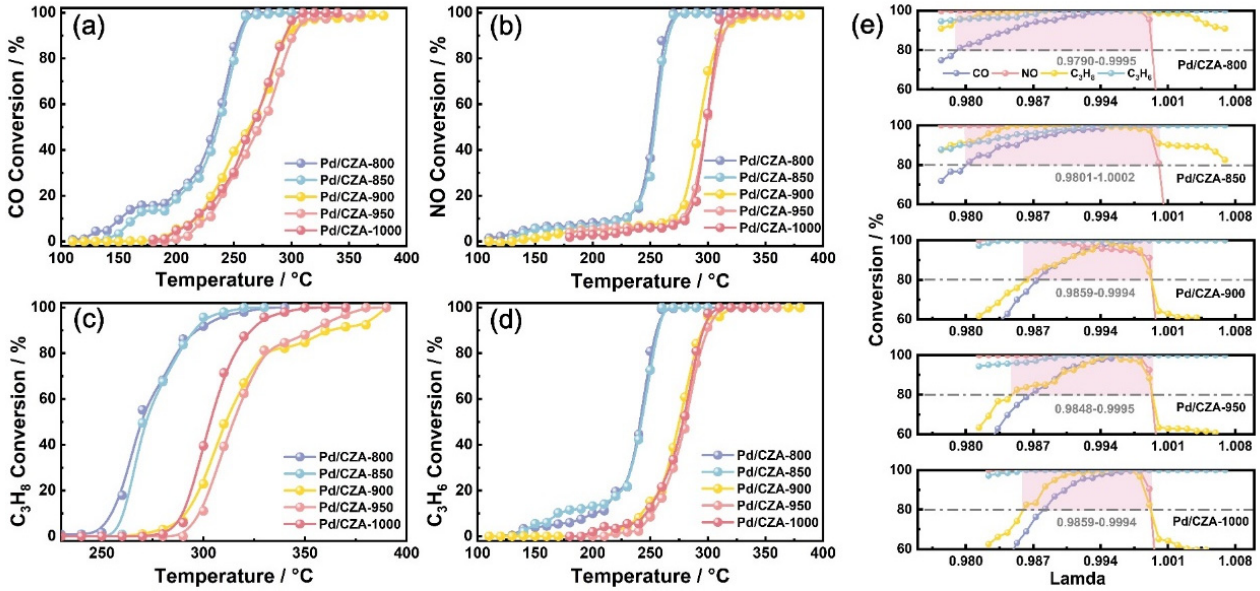

Fig. 1 Light-off curves of (a) CO, (b) NO, (c) C_3H_8 and (d) C_3H_6; (e) Operation windows of the aged catalysts

Simulated exhaust gas consisted of 4500 μL/L CO, 1200 μL/L NO, 120 μL/L C_3H_8, 220 μL/L C_3H_6, 3130 μL/L O_2, 1500 μL/L H_2, 110 mL/L CO_2, 100 mL/L H_2O, and N_2 as the balance gas. Operation window was tested at 400 ℃. Colorful figures are available on website

Table 1 T_{50} and T_{90} values of CO, NO and HCs of the aged catalysts

Sample	CO		NO		C_3H_8		C_3H_6	
	T_{50}/℃	T_{90}/℃	T_{50}/℃	T_{90}/℃	T_{50}/℃	T_{90}/℃	T_{50}/℃	T_{90}/℃
Pd/CZA-800	233	254	252	263	269	297	241	255
Pd/CZA-850	237	256	254	266	271	295	242	256
Pd/CZA-900	263	295	292	310	311	362	275	295
Pd/CZA-950	272	302	298	313	314	353	280	300
Pd/CZA-1000	265	295	298	310	303	324	278	295

The operating window of a TWC is defined by the air-fuel ratio (λ) range enabling ≥80% simultaneous conversion of NO, CO and HCs, which is a key indicator of its adaptability to fluctuating exhaust conditions. As shown in Fig. 1(e), Pd/CZA-800 and Pd/CZA-850 exhibit significantly wider operating windows than other catalysts, while the window of Pd/CZA-900 narrows sharply. This indicates its poorer tolerance to fluctuations in the air-fuel ratio. The abrupt shift in activity and operating window indicates that both microchemical state of Pd and MSI undergo significant changes in the range of 850–900 ℃ since the support has been pretreated at high temperature. The factors contributing to the marked contrast in activity between Pd/CZA-850 and Pd/CZA-900 are expounded in subsequent sections.

2.2 Textural properties of catalysts

The textural properties of the catalysts were assessed through physical adsorption-desorption and XRD analyses, as detailed in Table 2. The specific surface area of Pd/CZA catalysts exhibits a slight increase with the aging temperature, yet remains relatively stable, which is ascribed to the pretreatment of the CZA support at 1000 ℃. Consequently, the subsequent high-temperature aging has minimal impact on the specific surface area of catalysts. The slight increase in specific surface area may be attributed to pore reorganization caused by elevated temperatures. Similarly, the pore volume and average pore size of the catalysts exhibit insignificant changes. These results indicate that the specific surface area of the catalyst is no longer a key factor influencing its catalytic activity.

Table 2 Textural properties of catalysts

Sample	S_{BET}/($m^2 \cdot g^{-1}$)	Pore volume/($mL \cdot g^{-1}$)	Average pore size/nm
Pd/CZA-800	61	0.44	23.2
Pd/CZA-850	67	0.42	24.5
Pd/CZA-900	67	0.41	24.7
Pd/CZA-950	69	0.43	24.6
Pd/CZA-1000	70	0.40	29.1

2.3 Pd-CZA interaction and Pd microchemical states

2.3.1 Redox property and metal-support interaction

Hydrogen temperature-programmed reduction (H_2-TPR) was used to evaluate the redox properties of the Pd/CZA catalysts, as depicted in Fig. 2(a). All catalysts exhibit three primary peaks α, β and γ, associated with the decomposition of PdH_x[25], the reduction of isolated PdO_x[9] and the reduction of Ce^{4+} which has a strong interaction with Pd[26], respectively. Typically, the PdH_x decomposition peak is related to the size of Pd particles, with larger Pd particles exhibiting a higher tendency to form PdH_x[27]. The more prominent negative peak observed in catalyst aged at 900 ℃, suggesting the formation of larger Pd particles. The significant enhancement of the β peak on Pd/CZA-900 indicates a larger amount of reducible PdO_x species. These PdO_x exist as an isolated form rather than being bonded to the support, signifying weaker MSI.

The decomposition temperature of PdO_x within the Pd/CZA catalyst was determined using oxygen temperature-programmed desorption (O_2-TPD), as depicted in Fig. 2(b). The desorption peak at approximately 200 ℃ corresponds to the removal of surface-adsorbed oxygen on the ceria-zirconia solid solution, while the peak at around 700 ℃ signifies the decomposition of PdO_x[28]. A comparison between Pd/CZA-850 and Pd/CZA-900 reveals a decrease in the decomposition temperature of PdO_x from 785 to 669 ℃, indicating a notable weakening of the interaction between Pd and CZA support in Pd/CZA-900. This weakened interaction prevents the support from stabilizing PdO_x, thereby promoting its decomposition. Furthermore, the desorption peak area of PdO_x in the Pd/CZA-900 catalyst substantially increases, demonstrating that aging at 900 ℃ leads to agglomerated PdO_x particles with reduced support contact and weakened Pd–O–Ce bond, which is consistent with the above-mentioned H_2-TPR results.

XPS was used to characterize the chemical states of Pd in different catalysts. By deconvoluting the fine spectra of $Pd3d_{5/2}$, the relative concentrations of Pd^0 and Pd^{2+} on the catalyst surfaces were determined. As shown in Fig. 2(c-g), Pd^0 is identified at ~340.4 eV and Pd^{2+} at ~342.0 eV, with some overlap peak observed between Zr3p and Pd3d[29]. Among Pd/CZA-900 and Pd/CZA-950, Pd^{2+} has higher binding energy than other catalysts, indicating higher oxidation state and greater difficulty in reduction. The surface Pd^{2+} ratios ($Pd^{2+}/(Pd^0+Pd^{2+})$) for Pd/CZA catalysts aged at temperatures ranging from 800 to 1000 ℃ are 72.56%, 74.71%, 83.19%, 80.03% and 81.61%, respectively. The higher Pd^{2+} content in Pd/CZA-900 is consistent with the increased PdO_x reduction peak observed in H_2-TPR.

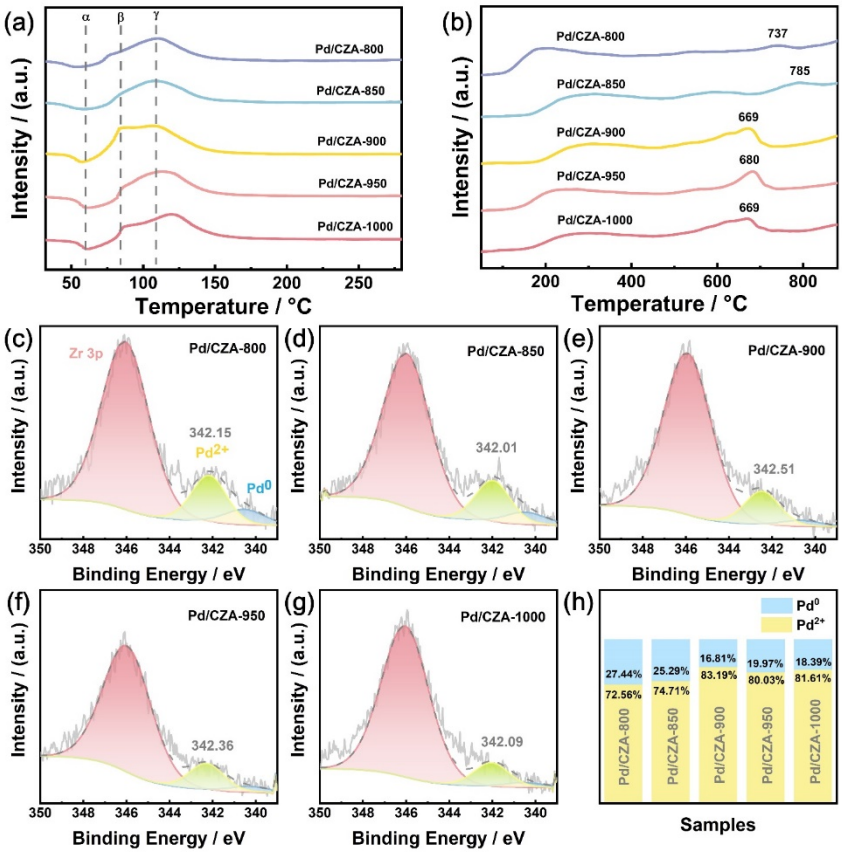

Fig. 2 (a) H_2-TPR curves, (b) O_2-TPD curves, (c-g) Pd3d XPS spectra and (h) Pd species ratio of the catalysts

2.3.2 Structural property and Pd particle size

High-resolution transmission electron microscopy (HRTEM) was employed to characterize the microstructure of the catalysts and the aggregation state of Pd species. Due to the low contrast between Pd and CZ, the specific species forming the aggregates cannot be identified, making it impossible to statistically determine the particle size distribution of Pd from these results. However, regardless of whether the aggregated particles are Pd or CZ, the high temperature of 900 ℃ evidently disrupts the well-dispersed state of particles, leading to severe sintering. As shown in Fig. 3(a-c), lattice fringe corresponding to Pd (111) with a spacing of 0.26 nm is observed in three catalysts. However, this characteristic region is not distinctly observed in either Pd/CZA-800 or Pd/CZA-850. Detailed TEM images are showen in Fig. S1 and Fig. S2.

As shown in Fig. 3(d), XRD patterns indicates a strong correlation between the primary diffraction peaks of the Pd/CZA catalyst and the characteristic peaks of $Ce_{0.5}Zr_{0.5}O_2$ (PDF#38-1436)[30]. Furthermore, a minor diffraction peak at 67.3° can be attributed to Al_2O_3. Notably, a subtle characteristic peak of PdO species appears at 54.7° in catalysts aged at 900 ℃ and above, while no distinct diffraction peaks of Pd species are observed in Pd/CZA-800 and Pd/CZA-850[27]. This suggests that Pd species undergo minimal sintering after aging at temperatures up to 850 ℃. Nevertheless, elevating the aging temperature to 900 ℃ prompts rapid agglomeration and sintering of Pd species into larger particles, resulting in a significant decrease in catalytic activity.

The assessment of CO adsorption capacity using pulsed CO chemisorption is a reliable technique for evaluating Pd dispersion and particle size, which are crucial factors influencing catalytic activity. High dispersion of noble metals leads to enhanced accessibility of active sites, promoting the adsorption and activation of reactants, thereby boosting catalytic performance[31]. The results are depicted in Fig. 3(e). Evidently, Pd dispersion and particle size are comparable between Pd/CZA-800 and Pd/CZA-850, both demonstrating well-dispersed Pd. In contrast, Pd dispersion decreases from 37.34% to 13.29%, and particle size increases from 2.9 to 8.2 nm in Pd/CZA-900, indicating pronounced sintering of Pd into larger particles after aging at 900 ℃. The results for Pd/CZA-900, Pd/CZA-950 and Pd/CZA-1000 exhibit fluctuations similar to the activity performance, although with minor differences, all exhibit low Pd dispersion and large Pd particle sizes. Overall, with increasing aging temperature, Pd dispersion decreases and Pd particle size increases, showing a marked transition in the range of 850–900 ℃.

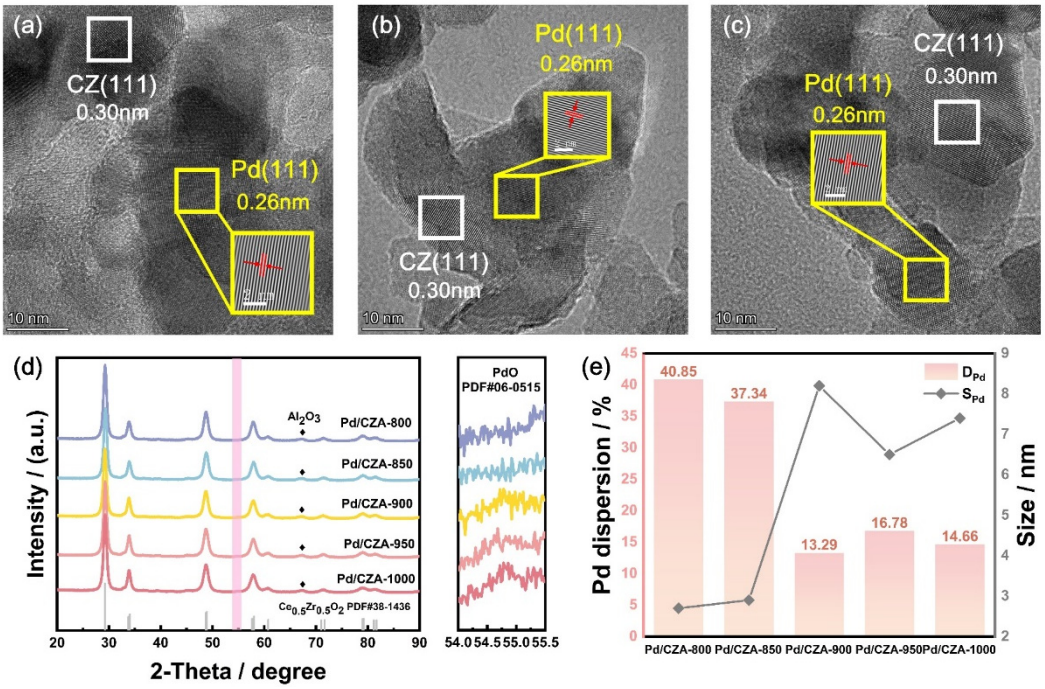

Fig. 3 HRTEM images of (a) Pd/CZA-900, (b) Pd/CZA-950, and (c) Pd/CZA-1000; (d) XRD patterns of the catalysts and partial enlarged view of the pink area; (e) Pd dispersion and particle size of the catalysts

These findings suggest that aging at 900 °C weakens the MSI, leading to agglomeration of Pd particles into larger PdO_x clusters. The agglomeration reduces the number of active sites, resulting in a decrease in catalytic activity.

2.4 Adsorption and activation capacity for C_3H_8 and O_2

The dynamic oxygen storage capacity (DOSC) test can evaluate how the catalysts interact with oxygen[32]. Fig. 4(a) illustrates the temporal evolution of oxygen storage and release capacities for different catalysts, alongside the corresponding CO_2 production rate as shown in Fig. 4(b). The sharp decline in the CO_2 production rate for the Pd/CZA-900 indicates a reduced rate of active oxygen migration, resulting in compromised efficiency of the Ce redox cycle and reduced catalytic performance. This behavior can be attributed to the presence of larger PdO_x species in Pd/CZA-900, which reduces the density of active sites and impairs oxygen adsorption and activation capabilities.

The activity of oxygen species on the catalyst was further evaluated using TG analysis under alternating H_2/O_2 atmospheres at 100 °C. The mass change profiles of the catalysts are depicted in Fig. 4(c). Specifically, the duration required for the mass to reach an equilibrium state during the redox cycle was analyzed[33]. The findings reveal that Pd/CZA-800 and Pd/CZA-850 exhibit rapid weight loss under H_2 atmosphere within 14 min, followed by swift mass recovery upon exposure to O_2. In contrast, for Pd/CZA-900 and beyond, the time taken for weight loss to stabilize in H_2 notably extends to 30 min, indicating constrained oxygen diffusion on these catalysts, which impedes the efficacy of the redox cycling process. These observations align with the results of the dynamic oxygen storage capacity.

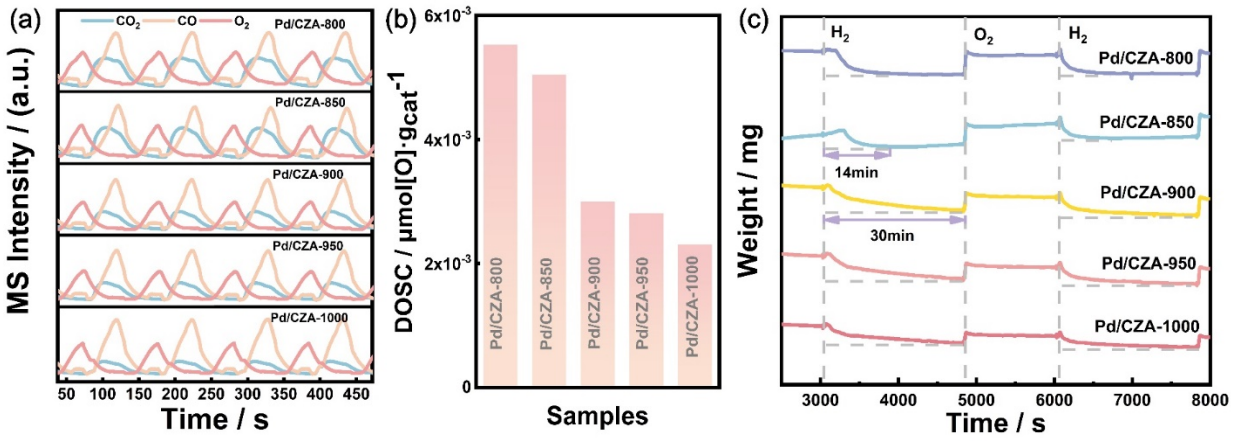

Fig. 4 (a) DOSC profiles of CO-O_2 alternating pulse, (b) DOSC values and (c) H_2-O_2 atmosphere alternating TG curves of the

catalysts

Colorful figures are available on website

In order to characterize the adsorption and activation ability of the catalyst for reactants, C_3H_8-TPD coupled with mass spectrometry (MS) was used to monitor desorption products during the heating process after C_3H_8/N_2 adsorption, as illustrated in Fig. 5(a). No MS signal for C_3H_8 is observed because the physical adsorption energy is very low on the stoichiometric or defect surface due to the non-polar characteristic of propane[34]. Concurrently, the formation of CO_2 (m/z=44) arising from the reaction between chemisorbed propane and subsurface lattice oxygen of the catalyst is tracked throughout the heating process. As shown in Fig. 5(b), the CO_2 peak intensities of Pd/CZA-800 and Pd/CZA-850 are relatively high at about 200 ℃, and the peak intensity decreases significantly from Pd/CZA-900, indicating that the active oxygen species of the catalyst and the ability of adsorption and activation for C_3H_8 decrease with increasing aging temperature to 900 ℃, which is consistent with other characteristics mentioned above.

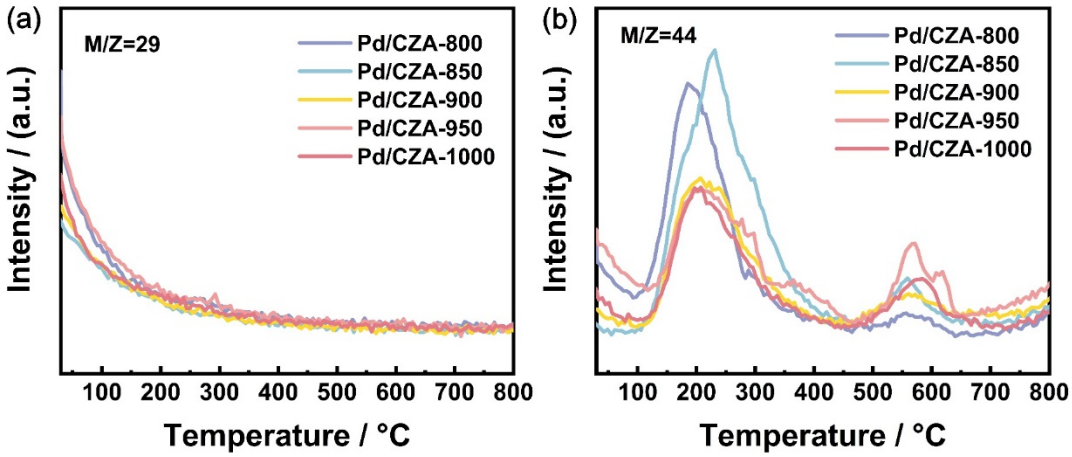

Fig. 5 (a) C_3H_8 and (b) CO_2 desorption signals of C_3H_8-TPD over the catalysts

Colorful figures are available on website

2.5 Structure-activity relationship discussion

Fig. 6 illustrates the structure-activity relationship of the catalyst. For the Pd/CZA TWCs studied, the activities of Pd/CZA-800 and Pd/CZA-850 are essentially identical, while the activities of Pd/CZA-900, Pd/CZA-950 and Pd/CZA-1000 exhibit minimal differences. However, a significant activity discontinuity is observed between Pd/CZA-850 and Pd/CZA-900. Comprehensive characterization reveals that this abrupt activity decline stems from a drastic change in the microchemical state of Pd with increasing aging temperature.When the aging temperature reaches 900 ℃, the MSI is significantly weakened. Consequently, Pd can no longer be effectively anchored onto the CZA support, leading to its migration and aggregation into larger Pd clusters.

These larger Pd species exhibit substantially reduced capability for adsorbing and activating reactants and oxygen, impeding the efficient redox reaction process, ultimately resulting in the observed plummeting TWC activity. Firstly, results from N_2 adsorption-desorption rule out the possibility of structural collapse of the support at high temperatures embedding active sites. Secondly, H_2-TPR, XPS, and O_2-TPD results demonstrate a significant weakening of the MSI in Pd/CZA-900. Pd species deprived of the stabilizing Pd–O–Ce bonds migrate, forming larger isolated particles, while decreasing the decomposition temperature of PdO. Subsequently, XRD, CO chemisorption, and HRTEM results corroborate the reduction in Pd dispersion and the increase in Pd particle size. H_2-O_2/TG and DOSC results confirm a diminished oxygen response capability in Pd/CZA-900. Both oxygen transport and redox cycling are inhibited. Finally, C_3H_8-TPD results also indicate a markedly reduced ability of Pd/CZA-900 to adsorb and activate C_3H_8, leading to a rapid decline in the conversion efficiency of reactants.

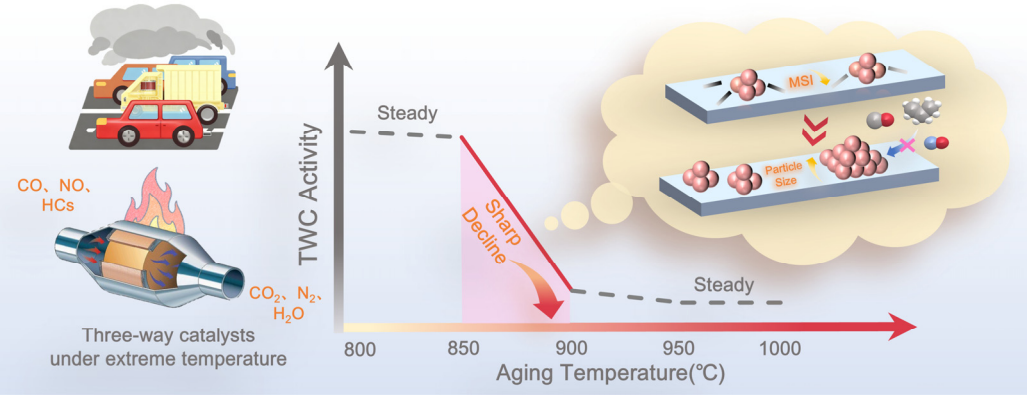

Fig. 6 Schematic diagram of structure-activity relationship

3 Conclusions

In this study, a series of Pd/CZA catalysts aged at temperatures of 800–1000 ℃ are prepared to systematically assess their catalytic performance. The findings reveal a decline in the TWC activity of Pd/CZA with increasing aging temperature, with a notable decrease observed between Pd/CZA-850 and Pd/CZA-900. Specifically, there is a sharp decrease in TWC activity at 900 ℃ aging temperature, as evidenced by increases of 26–40 ℃ and 39–67 ℃ in the T_{50} and T_{90} for CO, NO and HCs, respectively. Various characterizations suggest that Pd–O–Ce bond is significantly weakened at aging temperature 900 ℃ and above, leading to the inability of the support to maintain the dispersion of Pd species. Consequently, larger Pd particles form, resulting in diminished capacity for adsorbing and activating reactants and oxygen, which hinders effective redox cycling and pollutant conversion processes. This work demonstrates that the TWC activity of Pd/CZA exhibits a nonlinear decay at high temperatures, which is attributed to a change in the microchemical state of Pd occurring at 900 ℃ aging. By correlating aging temperature with the evolution of Pd state, this study deepens the understanding of thermal deactivation mechanisms in Pd-based catalysts and offers a practical guidance for designing catalysts with high thermal stability.

Supporting Materials

Supporting materials related to this article can be found at https://doi.org/10.15541/jim20250396.

References

[1] FARRAUTO R J, DEEBA M, ALERASOOL S. Gasoline automobile catalysis and its historical journey to cleaner air. *Nature Catalysis*, 2019, **2:** 603.

[2] JOSHI A. Year in review: progress towards decarbonizing transport and near-zero emissions. *SAE Technical Paper Series*, DOI: 10.4271/2023-01-0396.

[3] JOSHI A. Review of vehicle engine efficiency and emissions. *SAE International Journal of Advances and Current Practices in Mobility*, **4(5):** 1704.

[4] WANG J H, CHEN H, HU Z C, *et al*. A review on the Pd-based three-way catalyst. *Catalysis Reviews*, 2015, **57(1):** 79.

[5] MARTÍN A J, MITCHELL S, MONDELLI C, *et al*. Unifying views on catalyst deactivation. *Nature Catalysis*, 2022, **5:** 854.

[6] MORIKAWA A, SUZUKI T, KANAZAWA T, *et al*. A new concept in high performance ceria-zirconia oxygen storage capacity material with Al_2O_3 as a diffusion barrier. *Applied Catalysis B*: *Environmental*, 2008, **78(3/4):** 210.

[7] MAMONTOV E, EGAMI T, BREZNY R, *et al*. Lattice defects and oxygen storage capacity of nanocrystalline ceria and ceria-zirconia. *The Journal of Physical Chemistry B*, 2000, **104(47):** 11110.

[8] KEITL G, RINK J, WEN F, *et al*. Impact of test conditions on the oxygen storage capacity of Pd loaded cerium zirconium oxide. *Topics in Catalysis*, 2017, **60(3):** 272.

[9] DING Y Q, WU Q Q, LIN B, *et al*. Superior catalytic activity of a Pd catalyst in methane combustion by fine-tuning the phase of ceria-zirconia support. *Applied Catalysis B*: *Environmental*, 2020, **266:** 118631.

[10] FAN J, CHEN L L, LI S S, *et al*. Insights into the promotional effect of alkaline earth metals in Pt-based three-way catalysts for NO reduction. *Journal of Catalysis*, 2023, **418:** 90.

[11] WOO H, LEE E J, PARK H, *et al*. Enhancing the thermal stability and activity of Pd-Rh/Al_2O_3 catalyst for three-way catalytic reaction by introducing Pt and varying the synthesis

method. *Journal of Environmental Chemical Engineering*, 2023, **11(5):** 110671.

[12] CHALLA S R, DELARIVA A T, HANSEN T W, *et al*. Relating rates of catalyst sintering to the disappearance of individual nanoparticles during Ostwald ripening. *Journal of the American Chemical Society*, 2011, **133(51):** 20672.

[13] VEDYAGIN A A, VOLODIN A M, KENZHIN R M, *et al*. Characterization and study on the thermal aging behavior of palladium-alumina catalysts. *Journal of Thermal Analysis and Calorimetry*, 2017, **130(3):** 1865.

[14] MUTA T, OHTA R, TSUSHIDA M, *et al*. Rh/Al_2O_3 and Pd/Al_2O_3 three-way catalysts show different thermal deactivation behaviors under real engine-aging conditions. *Catalysis Today*, 2025, **459:** 115422.

[15] KANG S B, LIM J B, JO D, *et al*. Ostwald-ripening sintering kinetics of Pd-based three-way catalyst: importance of initial particle size of Pd. *Chemical Engineering Journal*, 2017, **316:** 631.

[16] YAN S, ZHAO M, WANG J L, *et al*. The preparation of Pd/CeO_2-ZrO_2-Al_2O_3 catalyst with superior structural stability: effect of zirconia incorporation method. *Journal of Materials Science*, 2020, **55(23):** 9993.

[17] CHENG X M, ZHAO D P, ZHAO Y N, *et al*. Thermal deactivation mechanism of the commercial $Pt/Pd/Rh/CeO_2$-ZrO_2/Al_2O_3 catalysts aged under different conditions for the aftertreatment of CNG-fueled vehicle exhaust. *Fuel*, 2023, **344:** 128009.

[18] FUJIWARA A, TSURUNARI Y, YOSHIDA H, *et al*. Thermal deactivation of Pd/CeO_2-ZrO_2 three-way catalysts during real engine aging: analysis by a surface plus peripheral site model. *ACS Omega*, 2020, **5(44)**: 28897.

[19] YOSHIDA H, KAKEI R, FUJIWARA A, *et al*. Redox dynamics of Pd supported on CeO_2-ZrO_2 during oxygen storage/release cycles analyzed by time-resolved *in situ* reflectance spectroscopy. *The Journal of Physical Chemistry C*, 2018, **122(49):** 28173.

[20] VAN DEELEN T W, HERNÁNDEZ MEJÍA C, DE JONG K P. Control of metal-support interactions in heterogeneous catalysts to enhance activity and selectivity. *Nature Catalysis*, 2019, **2:** 955.

[21] SU S D, LI X M, LIU Z Y, *et al*. Microchemical environmental regulation of POMs@MIL-101(Cr) promote photocatalytic nitrogen to ammonia. *Journal of Colloid and Interface Science*, 2023, **646:** 547.

[22] CAO M, MAO Y J, WANG Q Q, *et al*. Sintering mechanism and sintering-resistant strategies for metal-based catalyst. *Chemical Industry and Engineering Progress*, 2023, **42(2):** 744.

[23] HANEDA M, NAKAMURA Y, YAMADA T, *et al*. Comprehensive study of the light-off performance and surface properties of engine-aged Pd-based three-way catalysts. *Catalysis Science & Technology*, 2021, **11(3):** 912.

[24] DATYE A K, VOTSMEIER M. Opportunities and challenges in the development of advanced materials for emission control catalysts. *Nature Materials*, 2021, **20(8)**: 1049.

[25] CHEN K, WAN J, LIN J S, *et al*. Comparative study of three-way catalytic performance over Pd/CeO_2-ZrO_2-Al_2O_3 and Pd/La-Al_2O_3 catalysts: new insights into microstructure and thermal stability. *Molecular Catalysis*, 2022, **526:** 112361.

[26] DENG J, CHEN Y S, LI M C, *et al*. Formation of partial κ-$Ce_2Zr_2O_8$ phase and its promotion on the supported Pd-only three-way catalysts. *Materials Research Bulletin*, 2021, **141:** 111341.

[27] WU B C, ZHANG Y L, YANG W H, *et al*. Insight into deactivation mechanism of Pd/Al_2O_3 catalyst during accelerated hydrothermal aging process. *Fuel*, 2025, **400:** 135707.

[28] YANG W H, WU Y, HUANG C S, *et al*. Magnesium-endowed exceptional hydrothermal stability of Pd/CeO_2-ZrO_2-Al_2O_3 catalyst for low-concentration methane combustion *via* two-step structure transformation. *Fuel*, 2024, **376:** 132743.

[29] WANG W, ZHOU Z W, WU B C, *et al*. Boosting the three-way catalytic reactions on Pd/CeO_2-ZrO_2-Al_2O_3 catalyst: the superior lanthanum-doping strategy. *Separation and Purification Technology*, 2025, **363:** 132294.

[30] JIANG X, FAN J, XIANG S Y, *et al*. Superior catalytic activity and high thermal durability of $MgAl_2O_4$ modified $Pt/Ce_{0.5}Zr_{0.5}O_2$ TWC. *Applied Surface Science*, 2022, **578:** 151915.

[31] ZHANG S, LI J, XIA Z M, *et al*. Towards highly active Pd/CeO_2 for alkene hydrogenation by tuning Pd dispersion and surface properties of the catalysts. *Nanoscale*, 2017, **9(9)**: 3140.

[32] SHEN M Q, WANG X Q, AN Y, *et al*. Dynamic oxygen storage capacity measurements on ceria-based material. *Journal of Rare Earths*, 2007, **25(1):** 48.

[33] SONG Z H, LIU X Z, QU L, *et al*. Construction of Pt^{2+}-O_v-Ce^{3+} enrooted structure by reduction-gel method to inhibit high

temperature deactivation of three-way catalysts. *Chemical Engineering Journal*, 2025, **522:** 167150.

[34] XIE Z A, YU T T, SONG W Y, *et al*. Highly active nanosized anatase TiO_{2-x} oxide catalysts *in situ* formed through reduction and Ostwald ripening processes for propane dehydrogenation. *ACS Catalysis*, 2020, **10(24):** 14678.

单钯三效催化剂在梯度温度老化下的失活机制

刘栩孜[1]，宋兆华[1]，曾 路[1]，屈 丽[2]，焦 毅[1]，蒋发军[3]，
李大成[3]，严会成[4]，王健礼[2]，陈耀强[2]

(1. 四川大学 新能源与低碳技术研究院，成都 610064; 2. 四川大学 化学学院，成都 610064; 3. 中自环保科技股份有限公司，成都 611731; 4. 四川蜀泰化工科技有限公司，遂宁 629300)

摘 要: 单 Pd/CZA 催化剂由第三代储氧材料 CeO_2-ZrO_2-Al_2O_3(CZA)与钯(Pd)构成，因其优异的污染物转化效率和抗烧结性能，成为一种更具实用性的汽油车三效催化剂(TWC)。尽管已有研究证实，Pd 基 TWC 的热失活机制与 Pd 颗粒烧结以及金属-载体相互作用(MSI)减弱密切相关，但其在极端高温条件下的热老化行为仍缺乏系统研究。本研究通过制备 800~1000 ℃温度老化的 Pd/CZA 催化剂，系统分析了其热失活过程，揭示了 Pd 微观化学状态随梯度老化温度的演变规律。利用一系列表征手段，评估了 Pd 微观化学状态及 MSI 与抗老化性能的关系。研究发现三效催化活性随老化温度的升高呈现出非线性衰减的趋势。在 850~900 ℃温度区间内，催化剂活性显著下降，一氧化碳(CO)、一氧化氮(NO)和碳氢化合物(HCs)的 T_{50} 与 T_{90}(污染物转化率达到 50%和 90%时的温度)分别升高了 26~40 ℃和 39~67 ℃; 而在 900~1000 ℃温度区间内, 催化活性变化不大。这种活性急剧下降的本质是 Pd 的微观化学状态发生了突变, 当老化温度升高至 900 ℃时，Pd–O–Ce 键变弱，导致 MSI 被削弱，Pd 颗粒失去对 Pd–O–Ce 的有效锚定，发生快速烧结和晶粒生长，从而明显阻碍反应物和氧气的吸附与活化过程。

关 键 词: 温度梯度；热老化；Pd-O-Ce 键；金属-载体相互作用；三效催化剂

中图分类号: O643 **文献标志码:** A **文章编号：**

Supporting materials

Deactivation Mechanism of Pd Only Three-way Catalysts under Aging Temperature Gradient

LIU Xuzi[1], SONG Zhaohua[1], ZENG Lu[1], QU Li[2], JIAO Yi[1], JIANG Fajun[3], LI Dacheng[3], YAN Huicheng[4], WANG Jianli[2], CHEN Yaoqiang[2]

(1. Institute of New Energy and Low-Carbon Technology, Sichuan University, Chengdu 610064, China; 2. College of Chemistry, Sichuan University, Chengdu 610064, China; 3. SINOTECH Company Limited, Chengdu 611731, China; 4. Sichuan Shutai Chemical Technology Co., Ltd., Suining 629300, China)

S1 Catalysts preparation

CeO_2-ZrO_2-Al_2O_3 (Solvay, pretreated at 1000 ℃ for 5 h, a specific surface area S_{BET} of 74 m^2/g) with a mass ratio of CeO_2 : ZrO_2 : Al_2O_3=3 : 3 : 4 was used as the support, and denoted as CZA. Pd-based catalysts (1 wt% Pd loading) were prepared by incipient wet impregnation. Firstly, 30 g CZA powder was added to $Pd(NO_3)_2$ solution (15.55% (in mass), 1.9293g) diluted with distilled water and vigorously stirred. After impregnation, the solution was dried at 60, 70 and 80 ℃ for 1 h respectively and calcination at 550 ℃ for 3 h. Subsequently, the above sample was divided into five parts and calcined at 800, 850, 900, 950 and 1000 ℃ for 5 h respectively, denoted as Pd/CZA-800, Pd/CZA-850, Pd/CZA-900, Pd/CZA-950 and Pd/CZA-1000.

The obtained catalyst powder was ball-milled into a slurry and then coated with cordierite honeycomb ceramic matrix (Corning, 2.5 cm^3, 400 cpsi (channels per square inch)) to prepare monolithic catalysts. The amount of coating was about 160 g/L.

S2 Catalysts characterizations

Autosorb SI automatic specific surface aperture analyzer (Quantachrome, USA) was used to analyze the textural properties of the catalysts. Prior to the test, the samples were pretreated under vacuum at 300 ℃ for 3 h, followed by N_2 absorption-desorption tests at liquid nitrogen temperature (77 K). Brunauer-Emmett-Teller (BET) and Barret Joyner-Halenda (BJH) methods were used to

calculate the specific surface area and pore volume.

Hydrogen temperature-programmed reduction (H_2-TPR) experiment was characterized on a programmed temperature controller equipped with a slender quartz tube reactor and a thermal conductivity detector (TCD, TP-5080D, Xianquan Co., Ltd, Tianjin, China). 100 mg catalyst was firstly processed at 450 ℃ for 30 min under He atmosphere to eliminate the influence of water and other impurities adsorbed on the surface, then cooled down to 30 ℃. After that, 5% H_2/N_2 (in volume) was introduced into the system with a flow rate of 30 mL/min. Finally, the sample was heated to 900 ℃ at a rate of 10 ℃/min, and the H_2 consumption signals were recorded by a TCD.

The elemental distribution on the surface was characterized by X-ray photoelectron spectroscopy (XPS), using XSAM-800 spectrometer (KRATOS, UK). The photoelectron is generated by the excitation of Al Kα X-ray, with a working voltage of 13 kV and a working current of 20 mA. The binding energy was calibrated using C1s (284.6 eV) as internal standard.

Oxygen temperature-programmed desorption (O_2-TPD) was performed on a programmed-temperature controller equipped with a fine quartz tube reactor and a TCD. The samples were pretreated in He atmosphere at 450 ℃ for 30 min, and then cooled to 30 °C. The sample was then adsorbed in 5 % O_2/N_2 (in volume) at 30 °C for 30 min. After saturation, the sample was heated up to 900 °C under He atmosphere at 10 °C/min and the signal was detected by a TCD.

The crystal structures of the catalysts were characterized by powder X-ray diffraction (XRD), which was performed on a Rigaku Ultima IV diffractometer (Rigaku Corporation, Japan). The X-ray tube was operated at 40 kV and 40 mA with a Cu Kα radiation (λ=1.5406 Å). The XRD patterns of samples were collected over the angular range of $20° \leq 2\theta \leq 90°$ with a scanning step size of 0.02°.

Pulse CO chemisorption was carried out to estimate the dispersion of Pd species by assuming CO : Pd=1 : 1. Prior to measurement, the sample was firstly pretreated in a pure H_2 flow at 450 ℃ for

40 min to reduce Pd species to the metallic state. It was then cooled to –78 ℃ in He flow to suppress the adsorption of CO onto Ce sites in the support. After that, CO was pulsed up to adsorption saturation and the component of effluent gas was monitored by a TCD. Based on the results of Pd dispersion, the size of Pd particles can be estimated as follows:

$$d_{Pd} = \frac{1.09}{D_{Pd}} \quad \text{(S1)}$$

where d_{Pd} is the size of Pd particles, and D_{Pd} is the dispersion degree of Pd particles.

The particle size and lattice fringes of catalysts were tested by a high-resolution transmission electron microscope (HRTEM, FEI Talos F200x, Thermo Scientific, USA) with an accelerating voltage of 200 kV.

The thermal analysis of the catalyst under alternating hydrogen-oxygen atmosphere was performed using thermogravimetry (Mettler-Toledo International Inc., Switzerland). The sample was evenly loaded into a crucible and heated to 100 ℃ in a flow of 99.999% N_2 (in volume, 50 mL·min^{-1}). The atmosphere was then switched to 21% O_2/N_2 (in volume, 50 mL·min^{-1}) for 20 min, followed by 5% H_2/N_2 (in volume, 50 mL·min^{-1}) for 30 min. This cyclic process was repeated two twice.

The dynamic oxygen storage capacity (DOSC) of sample was tested by using a cyclic multi-pulse adsorption (CO/O_2) experiment on a temperature-programmed adsorption/desorption apparatus (TP-5080D, Xianquan Co., Ltd., China) coupled with a mass spectrometer. 100 mg sample was pretreated in 2% O_2/Ar (in volume, 30 mL/min) at 450 ℃ for 40 min. This was followed by a 60 mL/min of CO/O_2 cyclic pulse test with a 140 mL/min of He flow as the carrier gas at 200 ℃. The test cycle lasted 100 s, consisting of 30 s of 4% CO/Ar (in volume, 60 mL/min) and 30 s of 2% O_2/Ar (in volume, 60 mL/min), with a 20 s interval between each gas injection. The calculation formula for DOSC is as follows:

$$DOSC = \frac{200 \times A \times 10^{-2} \times 10^{6}}{60 \times 22.4 \times 100} \quad (S2)$$

where A represents the average value of the integrated areas of 10 stable and consecutive CO_2 peaks.

C_3H_8-TPD was performed on a temperature programmed apparatus coupled with a mass spectrometer. 100 mg catalyst was pretreated at 450 ℃ under a He atmosphere with a flow rate of 30 mL·min^{-1} for 30 min and then cooledto 30 ℃. The sample was then adsorbed in 2% C_3H_8/N_2 (in volume) at 30 ℃ for 30 min. After saturation, the sample was heated up to 900 °C under He atmosphere at 10 °C/min and the signal was detected by a mass spectrometer.

S3 Catalytic activity tests

Catalytic activity tests on monolithic honeycomb catalysts were performed using a self-assembled fixed-bed continuous flow reactor under a stoichiometric atmosphere (air-fuel ratio $\lambda \approx 1$, as shown in Equation (S3)).The simulated exhaust gas consisted of 4500 μL/L CO, 1200 μL/L NO, 120 μL/L propane (C_3H_8), 220 μL/L propylene (C_3H_6), 3130 μL/L O_2, 1500 μL/L H_2, 110 mL/L CO_2 and 100 mL/L H_2O, and N_2 as the balance gas. The variations of reactants/products were monitored online by using a gas analyzer (Thermo Scientific, Antaris IGS). The gas hourly space velocity (GHSV) during the reactions was maintained at 50000 h^{-1}. Before the measurement, the catalysts were pretreated in the reaction mixture at 550 ℃ for 1 h. The concentration of each pollutant after catalytic conversion was detected under the condition of continuous temperature rise, and then the pollutant conversion curve with temperature change was obtained. The conversion (X) was calculated using Equation (S4). T_{50} and T_{90} (the temperatures at which the pollutant conversions are 50% and 90%, respectively) were recorded to evaluate catalytic activity.

$$\lambda = \frac{O_2 + 2CO_2 + CO + NO + H_2O}{2CO_2 + 2CO + 9C_3H_6 + 10C_3H_8 + H_2 + H_2O} \quad (S3)$$

$$X = \frac{C_{in} - C_{out}}{C_{in}} \times 100 \quad \text{(S4)}$$

Where O_2, CO_2, CO, *etc*. represent the concentrations of the respective substances, C_{in} represents the concentration of pollutants before entering the reactor, and C_{out} represents the concentration of pollutants discharged after passing through the reactor.

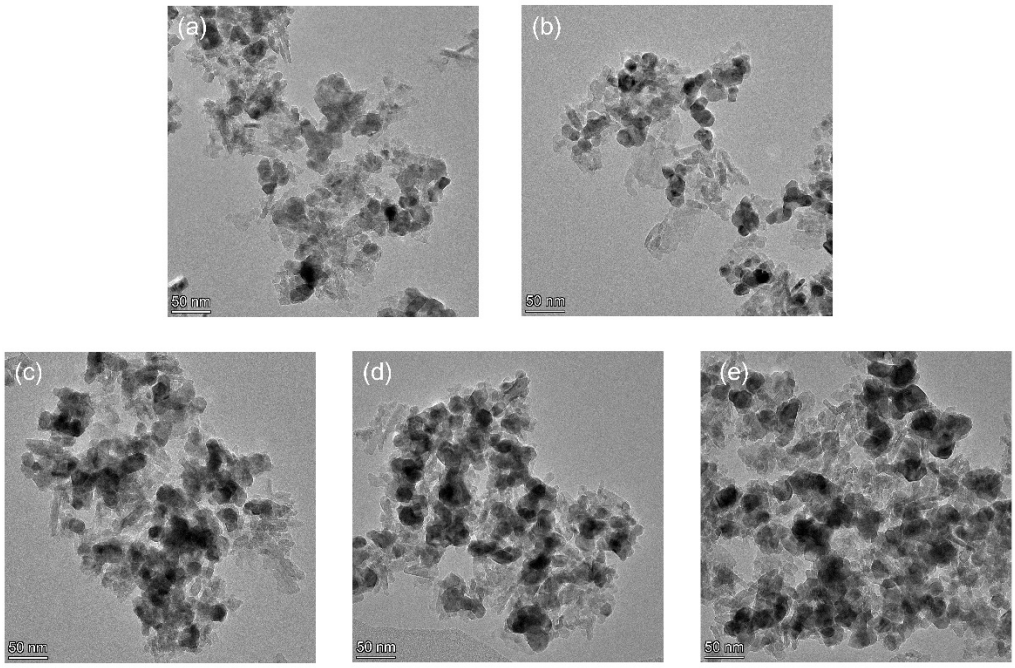

Fig. S1 TEM images of (a) Pd/CZA-800, (b) Pd/CZA-850, (c) Pd/CZA-900, (d) Pd/CZA-950 and (e) Pd/CZA-1000

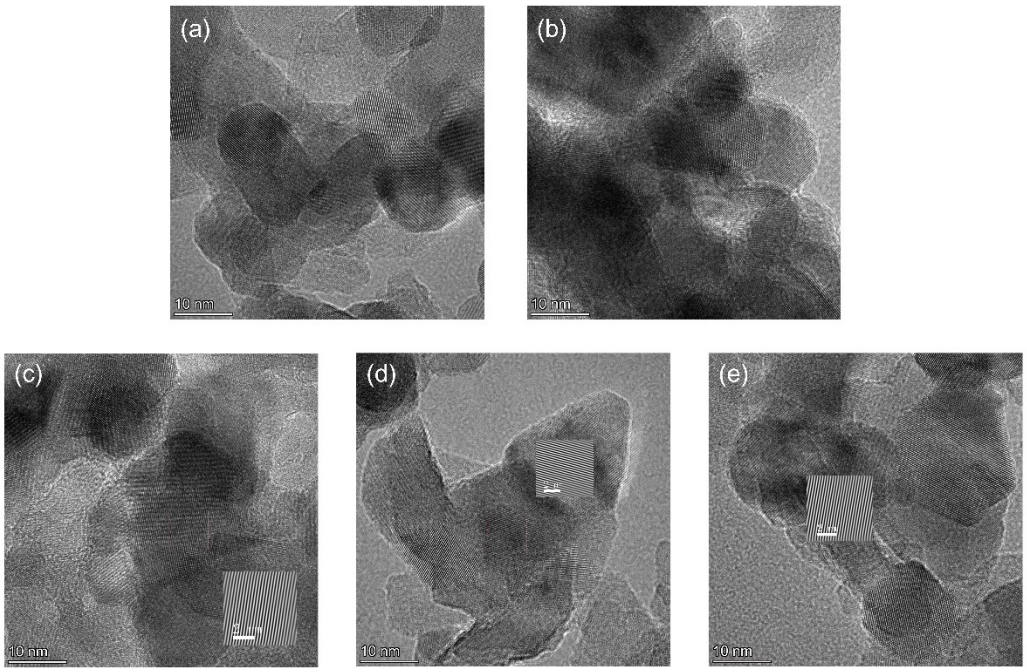

Fig. S2 HRTEM images of (a) Pd/CZA-800, (b) Pd/CZA-850, (c) Pd/CZA-900, (d) Pd/CZA-950 and (e)

Pd/CZA-1000